Mössbauer spectroscopy measurements on the 35.5 K superconductor $Rb_{1-\delta}EuFe_4As_4$

Mohammed A. Albedah,[1,2] Farshad Nejadsattari,[1] Zbigniew M. Stadnik,[1,*] Yi Liu,[3] and Guang-Han Cao[3]
[1]*Department of Physics, University of Ottawa, Ottawa, Ontario, Canada K1N 6N5*
[2]*Department of Physics, Majmaah University, P.O. Box 1712, Zulfi, Saudi Arabia*
[3]*Department of Physics, Zhejiang University, Hangzhou 310027, China*

(Received 23 February 2018; revised manuscript received 14 April 2018; published 30 April 2018)

The results of x-ray diffraction and ^{57}Fe and ^{151}Eu Mössbauer spectroscopy measurements, supplemented with *ab initio* hyperfine-interaction parameter calculations, on the new 35.5 K superconductor $Rb_{1-\delta}EuFe_4As_4$ are presented. The superconductor crystallizes in the tetragonal space group $P4/mmm$ with the lattice parameters $a = 3.8849(1)$ Å and $c = 13.3370(3)$ Å. It is shown that there is no magnetic order of the Fe magnetic moments down to 2.1 K and that the ferromagnetic order is associated solely with the Eu magnetic moments. The Curie temperature $T_C = 16.54(8)$ K is determined from the temperature dependence of both the hyperfine magnetic field at ^{151}Eu nuclei and the transferred hyperfine magnetic field at ^{57}Fe nuclei that is induced by the ferromagnetically ordered Eu sublattice. The Eu magnetic moments are demonstrated to be perpendicular to the crystallographic c axis. The temperature dependence of the principal component of the electric field gradient tensor, at both Fe and Eu sites, is well described by a $T^{3/2}$ power-law relation. Good agreement between the calculated and measured hyperfine-interaction parameters is observed. The Debye temperature of $Rb_{1-\delta}EuFe_4As_4$ is found to be 391(8) K.

DOI: 10.1103/PhysRevB.97.144426

I. INTRODUCTION

Discovered in 2016, $AeAFe_4As_4$ (Ae = Ca, Sr, Eu and A = K, Rb, Cs) compounds are a new Fe-based class of superconductors with the critical temperature T_c in the range 31.6–36.8 K [1–4]. Unlike in solid solutions, such as intensively studied $(Ba_{1-x}K_x)Fe_2As_2$ or $(Sr_{1-x}Na_x)Fe_2As_2$, the Ae and A atoms in $AeAFe_4As_4$ occupy crystallographically inequivalent positions, which changes the space group from $I4/mmm$ to $P4/mmm$. The crystal structure of these new superconductors consists of the Ae and A layers alternately stacked along the crystallographic c axis between the Fe_2As_2 slabs. Therefore, these fully ordered, stoichiometric Fe-based superconductors offer a unique opportunity to study, among other things, the relation between superconductivity and possible long-range magnetic order.

The superconductor $RbEuFe_4As_4$ with a critical superconducting temperature $T_c = 36.5$ K exhibits an anomaly at ~15.0 K in the magnetic-susceptibility and specific-heat data [3]. The isothermal magnetization measurements allowed the identification of this anomaly as a ferromagnetic transition [3]. The ferromagnetism in the $RbEuFe_4As_4$ superconductor has been suggested [3] to result from the ordering of the Eu magnetic moments. This is equivalent to assuming that the Fe atoms in $RbEuFe_4As_4$ carry no magnetic moment. No orientation of the magnetic moment in $RbEuFe_4As_4$ with respect to the crystallographic axes has been established.

The main goal of this study is to determine whether the magnetic moment in the $RbEuFe_4As_4$ superconductor is associated with only Eu or Fe atoms or with Eu and Fe atoms and what its orientation is relative to the crystallographic axes. To achieve this goal, ^{57}Fe and ^{151}Eu Mössbauer spectroscopy, supplemented by the first-principles calculations, will be utilized.

II. EXPERIMENTAL AND THEORETICAL METHODS

The $Rb_{1-\delta}EuFe_4As_4$ polycrystalline sample was prepared with a solid-state reaction method in an Ar atmosphere and at high temperatures, as described elsewhere [3].

An x-ray diffraction pattern was measured at 298 K in Bragg-Brentano geometry on a PANalytical X'Pert scanning diffractometer using Cu $K\alpha$ radiation in the 2θ range of 10°–120° in steps of 0.02°. The $K\beta$ line was eliminated by using a Kevex PSi2 Peltier-cooled solid-state Si detector. The chemical composition of the crystallites of the sample was determined using an energy-dispersive x-ray spectrometer (Model Octane Plus) equipped with a field-emission scanning electron microscope (Hitachi S-4800). The dc magnetization measurements were carried out using a Quantum Design magnetic property measurement system (MPMS-5).

The ^{57}Fe and ^{151}Eu Mössbauer measurements [5] were conducted using standard Mössbauer spectrometers operating in the sine mode, with sources ^{57}Co(Rb) and ^{151}Sm(SmF_3) at room temperature, respectively. The Mössbauer source ^{151}Sm(SmF_3) is not a monochromatic source as ^{151}Sm nuclei are located in the SmF_3 matrix at a site of noncubic symmetry. By measuring the ^{151}Eu Mössbauer spectra of a cubic EuSe compound, we determined that the electric quadrupole coupling constant [5] eQ_gV_{zz} [here e is the proton charge, $Q_g = 0.903$ b is the ground-state electric quadrupole moment of the ^{151}Eu nucleus [6], and V_{zz} is the principal component of the electric-field-gradient (EFG) tensor] in our source is −3.69(13) mm/s, which is close to the value of −3.6 mm/s

*stadnik@uottawa.ca

found in Ref. [7]. The precise shape of the source emission line was taken into account in the fits of the ^{151}Eu Mössbauer spectra.

The 14.4 and 21.5 keV γ rays were detected with a proportional counter. The spectrometers were calibrated with a 6.35-μm-thick α-Fe foil [8], and the spectra were folded. The Mössbauer absorbers consisted of a mixture of powder $Rb_{1-\delta}EuFe_4As_4$ and boron nitride, which was pressed into a pellet that was put into an 8-μm-thick Al disk container to ensure a uniform temperature over the whole absorber. The Mössbauer absorbers were put into a Mössbauer cryostat in which they were kept in a static exchange gas atmosphere at a pressure of $\sim 6\times10^{-3}$ mbar. The surface densities of the ^{57}Fe and ^{151}Eu Mössbauer absorbers were 17.23 and 29.1 mg/cm^2, respectively. They correspond to an effective thickness parameter t_a [5] of 2.96 f_a and 2.62 f_a, respectively (here f_a is the Debye-Waller factor of the absorber). Since $t_a > 1$, the resonance line shape of the Mössbauer spectra was described using a transmission integral formula [9]. The Mössbauer spectra at temperatures below the magnetic transition temperature were analyzed using a least-squares fitting procedure which entailed calculations of the positions and relative intensities of the absorption lines by numerical diagonalization of the full hyperfine interaction Hamiltonian.

Ab initio magnetic moment and Mössbauer hyperfine-interaction parameter calculations were performed within the framework of density functional theory using the full-potential linearized augmented plane wave plus local orbitals method as implemented in the WIEN2K package [10,11]. The experimental lattice parameters (a and c) and the atomic position parameters in the space group $P4/mmm$ (see below) were used in the calculations.

III. RESULTS AND DISCUSSION

A. Structural characterization

Figure 1 displays the room-temperature powder x-ray diffraction pattern of $Rb_{1-\delta}EuFe_4As_4$. The compound studied was shown [3] to crystallize in the tetragonal space group $P4/mmm$. A Rietveld refinement [12] of the x-ray powder diffraction data was carried out, yielding the lattice parameters $a = 3.8849(1)$ Å and $c = 13.3370(3)$ Å and the atomic positional parameters that are listed in Table I. We note (Fig. 1) that the specimen studied contains the second phases of FeAs [13] in the amount of 3.1(4) wt% and of Eu_2O_3 in the amount of 0.7(2) wt%. The values of a and c found here are, respectively, shorter and longer than the corresponding values in Ref. [3].

We found with energy-dispersive x-ray spectroscopy that the chemical composition of the crystallites studied was $Rb_{0.67(5)}EuFe_{4.1(7)}As_{4.3(5)}$. This indicates the existence of a significant Rb deficiency in the specimen. This deficiency induces an additional hole doping, which naturally explains the changes in the lattice parameters. The extra hole doping places the sample in an overdoped regime, which leads to a slight decrease of the superconducting transition temperature (see below).

The unit cell and the layered crystal structure of $RbEuFe_4As_4$ are shown in Fig. 2. The interactions between the Rb, Fe, and As atoms in the compound studied are depicted by various connecting rods. One observes that the layers of Eu

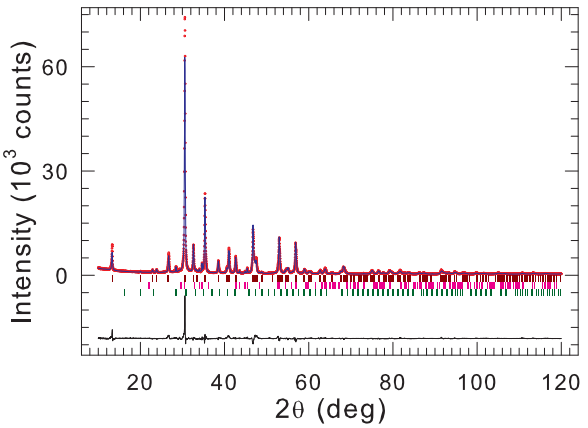

FIG. 1. Powder x-ray diffraction pattern of $Rb_{1-\delta}EuFe_4As_4$ at 298 K. The experimental data are denoted by open circles, while the line through the circles represents the results of the Rietveld refinement. The upper set of vertical dark red bars represents the Bragg peak positions corresponding to the $Rb_{1-\delta}EuFe_4As_4$ phase, the middle set of vertical pink bars corresponds to the positions of the impurity phase of FeAs (space group $Pnma$), and the lower set of vertical dark green bars refers to the positions of the impurity phase of Eu_2O_3 (space group $Ia\bar{3}$). The black solid line represents the difference curve between experimental and calculated patterns.

atoms are completely isolated from the Fe_4As_4 blocks and that two neighboring Fe_4As_4 blocks are separated by sheets of Rb atoms along the c direction.

The physical dimensions of the unit cell play an important role in some of the electronic transfer properties of the compound studied. In particular, each unit cell of $RbEuFe_4As_4$ is separated along the c direction from its neighboring cells by two planes formed by the Eu atoms. As a direct result of the elongation of the unit cell in the c direction, the $RbFe_4As_4$ units are practically isolated from the neighboring cells. Consequently, no direct electronic charge transfer between the neighboring $RbFe_4As_4$ units along the c direction is expected. Hence, one can consider the Eu layers to form barriers for the conduction electrons, forbidding them from freely propagating along the c direction. The absence of connecting rods in Fig. 2(b) between these layers of the Eu atoms and the $RbFe_4As_4$ units indicates this point. Thus, the insulating behavior of the compound studied along the c axis results from strong ionic interactions between the Eu layers and the $RbFe_4As_4$ units, leading to the charge delocalization that exists only within the $RbFe_4As_4$ units. In other words, the valence electrons of the Eu atoms are completely transferred to the $RbFe_4As_4$ units to form the aforementioned ionic couplings.

TABLE I. The Rietveld refined atomic positions for the tetragonal $RbEuFe_4As_4$ (space group $P4/mmm$).

Atom	Site	Point symmetry	Occupancy	x	y	z
Rb	1d	$4/mmm$	1.0	$\frac{1}{2}$	$\frac{1}{2}$	$\frac{1}{2}$
Eu	1a	$4/mmm$	1.0	0	0	0
Fe	4i	$2mm.$	1.0	0	$\frac{1}{2}$	0.2316(2)
As1	2g	$4mm$	1.0	0	0	0.3362(2)
As2	2h	$4mm$	1.0	$\frac{1}{2}$	$\frac{1}{2}$	0.1273(3)

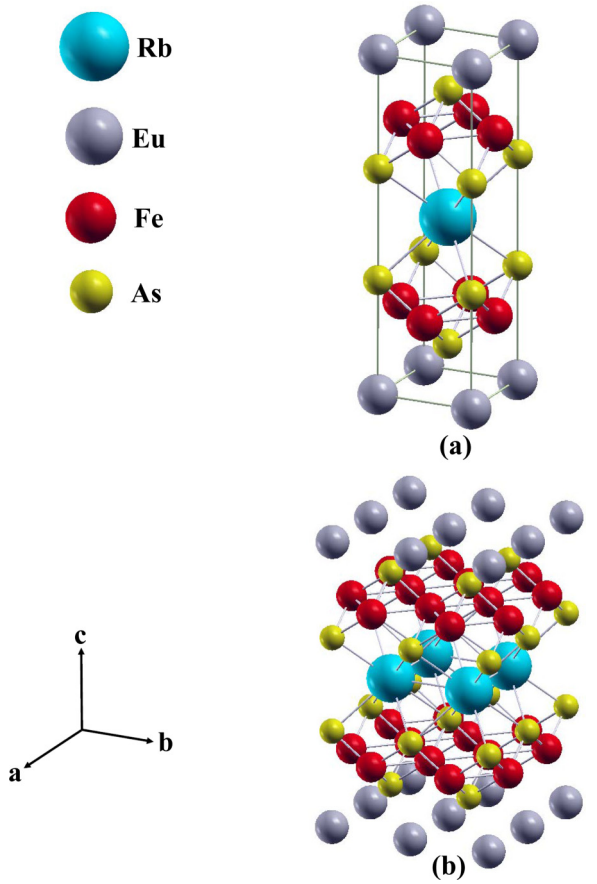

FIG. 2. (a) The unit cell and (b) the layered crystal structure of $RbEuFe_4As_4$.

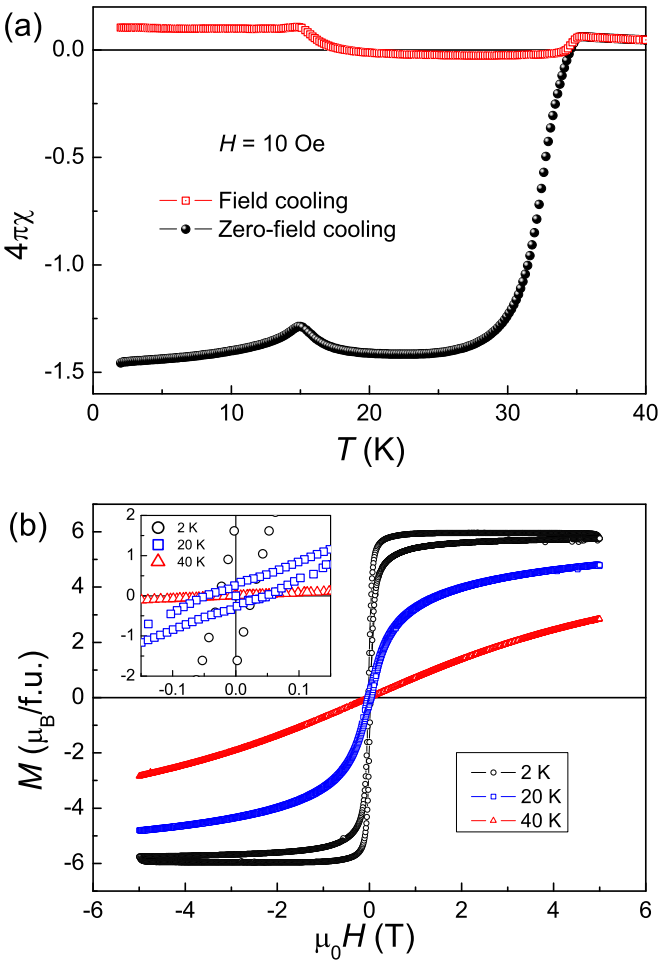

FIG. 3. (a) Temperature dependence of the field-cooled and zero-field-cooled dc magnetic susceptibility ($4\pi\chi$, in Gaussian units) of $Rb_{1-\delta}EuFe_4As_4$. (b) Field dependence of the magnetization of $Rb_{1-\delta}EuFe_4As_4$ at selected temperatures. The inset shows a close-up at low fields.

The tetragonal unit cell elongated along the c axis rules out the possibility of any strong interaction between the Eu layers. Therefore, no magnetic coupling is expected to exist between the Eu atoms along the c direction. One may thus predict that the interatomic interactions between the Eu atoms must occur in the ab plane and that a two-dimensional magnetic interaction mechanism, if any, between neighboring Eu atoms in each layer should exist.

B. Magnetic characterization

Superconductivity and ferromagnetism of the polycrystalline sample of $Rb_{1-\delta}EuFe_4As_4$ were verified by magnetic measurements. As shown in Fig. 3(a), bulk superconductivity is seen from the large magnetic shielding fraction (the volume fraction exceeds 100% because of the demagnetization effect). The superconducting transition temperature T_c is 35.5 K, 1 K lower than reported previously [3]. The slight decrease in T_c is probably due to the existence of the Rb deficiency (see above) that induces an overdoping effect.

The field-cooled magnetic susceptibility [Fig. 3(a)] shows an upturn below 20 K and levels off at $T_C = 15.0$ K, which is defined as the Curie temperature [3]. The anomalous magnetic response reflects the Eu-spin ferromagnetism, which is manifested by the isothermal magnetization shown in Fig. 3(b). Below T_C, an S-shaped magnetic hysteresis loop, one of the hallmarks of ferromagnetism, appears. The saturation magnetization of $6.0\,\mu_B$/f.u. is close to the value of $7.0\,\mu_B$/f.u. expected for full Eu^{2+}-spin ferromagnetism (the deviation might be due to the existence of the FeAs and Eu_2O_3 impurities in the sample studied). In fact, the hysteresis loop at 2.0 K is superposed by superconducting signals, as seen from the bifurcation of the magnetization at high fields [Fig. 3(b)]. At 20 K, the $M(H)$ loop mainly originates from type-II superconductivity with flux pinning and Brillouin-function-type paramagnetism. No magnetic hysteresis is observed at 40 K, consistent with the loss of ferromagnetism and superconductivity at that temperature. Thus, the data presented in Fig. 3 unambiguously confirm the presence of superconductivity and ferromagnetism below their respective transition temperatures in the $Rb_{1-\delta}EuFe_4As_4$ specimen.

C. Calculated magnetic moments and hyperfine interaction parameters

The calculated magnetic moments of the Rb, Eu, Fe, As1, and As2 atoms in ferromagnetic $RbEuFe_4As_4$ are $-0.0038\mu_B$, $6.7095\mu_B$, $1.1037\mu_B$, $-0.0688\mu_B$, and $-0.0857\mu_B$, respectively. It is thus predicted that the magnetism of $RbEuFe_4As_4$

is associated predominantly with the Eu atoms and to a lesser extent with the Fe atoms. A comparison between the calculated and experimental magnetic moments carried by the Eu and Fe atoms will be made below.

^{57}Fe Mössbauer spectra of a nonmagnetic compound or of a magnetically ordered compound at temperatures above its ordering temperature yield two important hyperfine-interaction parameters: the quadrupole splitting (the separation between two resonance lines in an ^{57}Fe Mössbauer quadrupole doublet) $\Delta = \frac{1}{2} eQ|V_{zz}|\sqrt{1+\eta^2/3}$, where Q is the electric quadrupole moment of the ^{57}Fe nucleus (0.15 b) [14] and η is the asymmetry parameter, and the isomer shift δ_0 [5]. For a crystalline compound of known crystal structure, V_{zz}, η, and δ_0 can also be obtained from *ab initio* calculations [15].

The calculated values of V_{zz} and η at the $4i$ site occupied by the Fe atoms (Table I) are 5.270×10^{20} V/m^2 and 0.8734, respectively. These values correspond to the predicted $\Delta = 0.0921$ mm/s.

The isomer shift $\delta_0 = \alpha[\rho(0) - \rho_{ref}(0)]$ results from the difference in the total electron density at the Mössbauer nucleus in the compound studied, $\rho(0)$, and in the reference compound, $\rho_{ref}(0)$; α is a calibration constant. In calculating $\rho(0)$, relativistic spin-orbit effects were invoked to account for the possibility of the penetration of the $p_{1/2}$ electrons into the ^{57}Fe nuclei. An α-Fe metal (with a bcc structure and a lattice constant of 2.8665 Å) was chosen as a reference compound. The calculated values of $\rho_{ref}(0)$ and $\rho(0)$ are 15309.905 and 15308.603 (a.u.)$^{-3}$, respectively. Using the calibration constant $\alpha = -0.291$ (a.u.)^3 (mm/s) [16], the calculated values of $\rho(0)$ and $\rho_{ref}(0)$ lead to $\delta_0 = 0.379$ mm/s.

Finally, the calculated hyperfine magnetic field at 0 K (Fermi contact term) at ^{57}Fe nuclei, $H_{hf}(0)$, is -56.2 kOe for ferromagnetic $RbEuFe_4As_4$. The Fermi contact term arises from a net spin-up and spin-down s-electron density at the nucleus as a result of spin polarization of inner filled s shells by spin-polarized partially filled outer shells [5,17].

The analysis of the ^{151}Eu Mössbauer spectra at different temperatures yields similar hyperfine-interaction parameters. The calculated values of V_{zz} and η at the $1a$ site occupied by the Eu atoms (Table I) are -49.659×10^{20} V/m^2 and 0.0, respectively. The $\eta = 0.0$ value is expected as the point symmetry $4/mmm$ of the $1a$ sites ensures an axially symmetric EFG tensor. The calculated $H_{hf}(0)$ at ^{151}Eu nuclei is 483 kOe for ferromagnetic $RbEuFe_4As_4$.

D. ^{57}Fe Mössbauer spectroscopy

^{57}Fe Mössbauer spectra of $Rb_{1-\delta}EuFe_4As_4$ at selected temperatures between room and liquid-helium temperatures were measured over a large velocity range (Fig. 4) in order to access the possibility of the presence of a Zeeman pattern resulting from a possible magnetic ordering of the Fe atoms in $Rb_{1-\delta}EuFe_4As_4$ and of a Zeeman pattern due to a magnetically ordered and Fe-containing impurity phase in the sample studied. A visual inspection of these spectra shows the absence of Zeeman patterns corresponding to the main and impurity phases with typical values of the hyperfine magnetic field H_{hf}. As will be shown in detail below, the large-spectral-area component of these spectra (Fig. 4) is due to $Rb_{1-\delta}EuFe_4As_4$ and is in the form of a quadrupole doublet with small Δ at

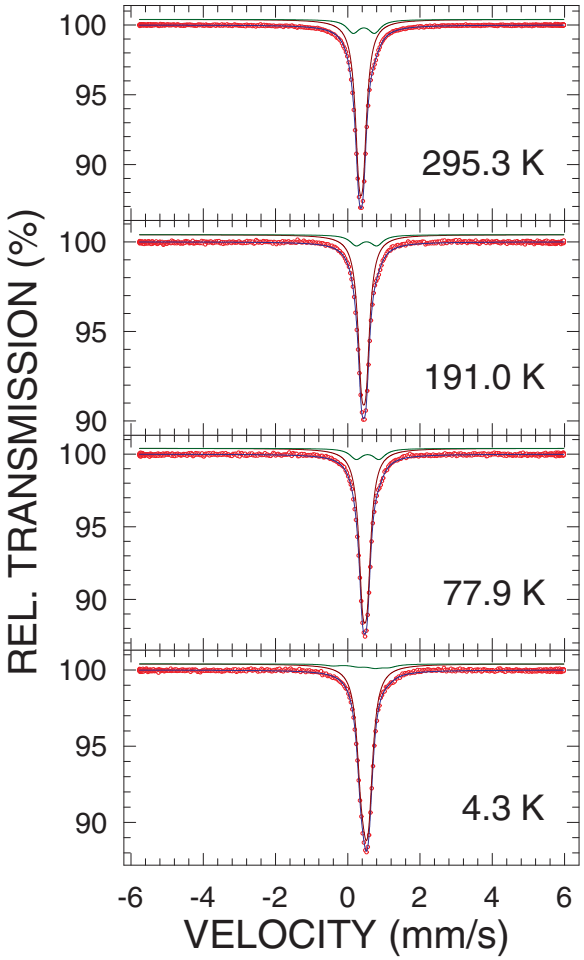

FIG. 4. ^{57}Fe Mössbauer spectra of $Rb_{1-\delta}EuFe_4As_4$ at selected temperatures measured over a large velocity range and fitted (solid blue lines) with a large-spectral-area quadrupole doublet at 295.3, 191.0, and 77.9 K and a Zeeman pattern at 4.3 K (solid dark red lines) due to $Rb_{1-\delta}EuFe_4As_4$ and with a small-spectral-area doublet at 295.3, 191.0, and 77.9 K and a Zeeman pattern at 4.3 K (solid dark green lines) due to the FeAs impurity phase, as described in the text. The zero-velocity origin is relative to α-Fe at room temperature.

295.3, 191.0, and 77.9 K and a Zeeman pattern with very small H_{hf} at 4.3 K. The small-spectral-area component of the spectra in Fig. 4 originates from the FeAs impurity phase and is in the form of a quadrupole doublet at 295.3, 191.0, and 77.9 K and a complex Zeeman pattern at 4.3 K.

Figure 5 shows the Mössbauer spectra of $Rb_{1-\delta}EuFe_4As_4$ at various temperatures down to the liquid-nitrogen temperature measured over a small velocity range. A feature on the right shoulder of the spectra indicates the presence of an impurity phase in the compound studied. Excellent fits of the spectra can be obtained with a large-spectral-area quadrupole doublet component with small Δ that originates from $Rb_{1-\delta}EuFe_4As_4$ and with a small-spectral-area quadrupole doublet component due to the FeAs impurity phase [18–20]. The spectral weight of the latter component, which is proportional to the product of the number of Fe atoms in the FeAs impurity and the Debye-Waller factor of the impurity, is 18(1)% and is larger than that expected from the amount of 3.1(4) wt% of the FeAs impurity derived from the x-ray diffraction spectrum.

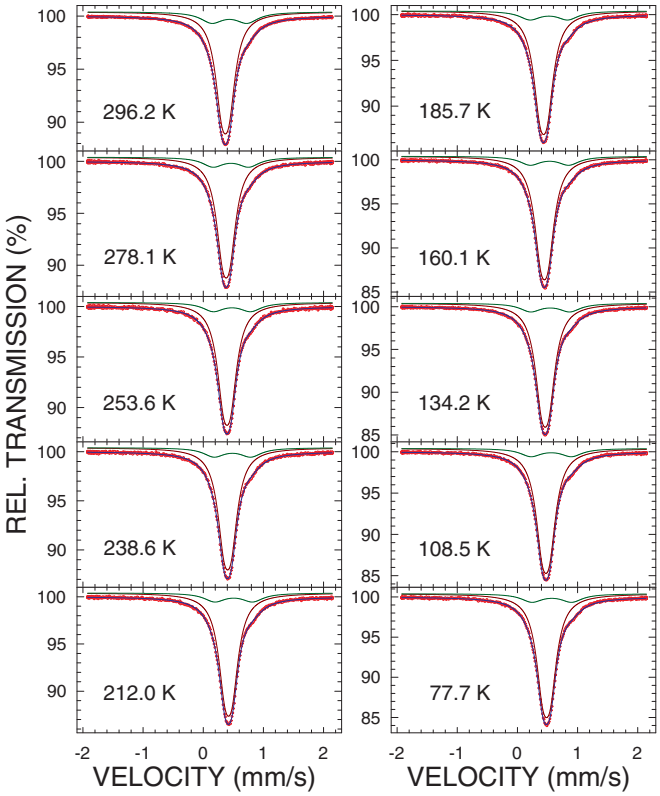

FIG. 5. ^{57}Fe Mössbauer spectra of $Rb_{1-\delta}EuFe_4As_4$ at the indicated temperatures fitted (solid blue lines) with a large-spectral-area quadrupole doublet due to $Rb_{1-\delta}EuFe_4As_4$ (dark red solid lines) and a small-spectral-area quadrupole doublet originating from the FeAs impurity phase (solid dark green lines), as described in the text. The zero-velocity origin is relative to α-Fe at room temperature.

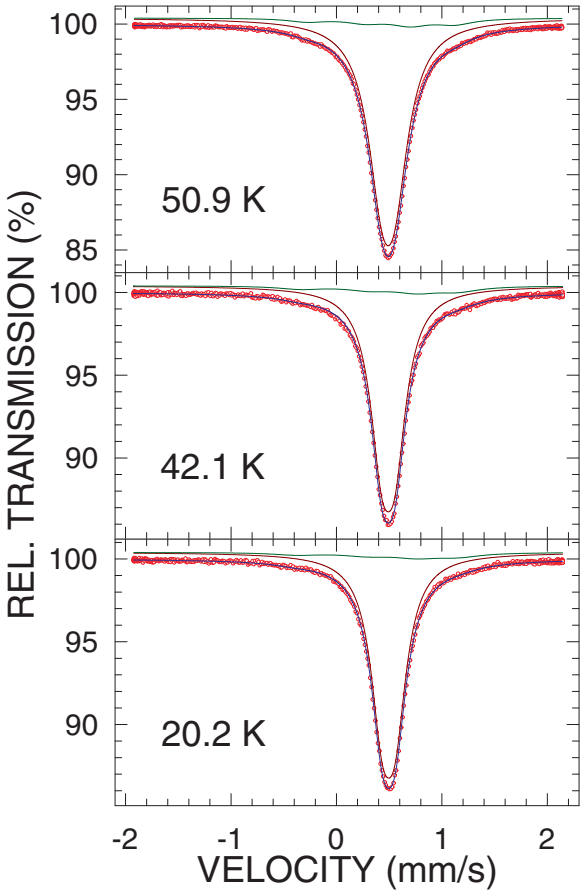

FIG. 6. ^{57}Fe Mössbauer spectra of $Rb_{1-\delta}EuFe_4As_4$ at the indicated temperatures fitted (solid blue lines) with a large-spectral-area quadrupole doublet due to $Rb_{1-\delta}EuFe_4As_4$ (dark red solid lines) and a small-spectral-area Zeeman pattern originating from the FeAs impurity phase (solid dark green lines), as described in the text. The zero-velocity origin is relative to α-Fe at room temperature.

A feature on the right shoulder of the spectra at temperatures below the liquid-nitrogen temperature (Fig. 6) disappears because the FeAs impurity component in these Mössbauer spectra is in the form of a complex Zeeman pattern. This indicates that the magnetic ordering temperature of the impurity phase lies in the range 77.7–50.9 K (Figs. 5 and 6). This agrees with the reported Néel temperature of FeAs (77(1) K in Ref. [13] and 69.2(1) K in Ref. [20]).

The temperature dependence of Δ obtained from the fits of the spectra in Figs. 5 and 6 is shown in Fig. 7(a). A small increase in Δ with decreasing temperature is observed. Such a temperature dependence of Δ has been observed in many metallic systems. It is well described by the empirical equation

$$\Delta(T) = \Delta(0)(1 - BT^{3/2}), \quad (1)$$

where $\Delta(0)$ is the value of Δ at 0 K and B is a constant. The fit of the $\Delta(T)$ data [Fig. 7(a)] to Eq. (1) gives $\Delta(0) = 0.1188(2)$ mm/s and $B = 10.1(8)\times10^{-6}$ K$^{-3/2}$. The value of B is similar to that found for a wide variety of other compounds, such as the ThFeAsN superconductor [21], crystalline approximants $Al_{76}Ni_9Fe_{15}$ [22] and $Al_{13}Fe_4$ [23] to quasicrystals, icosahedral $Al_{60}Cr_{19.9}Fe_{0.1}Ge_{20}$ [24] and decagonal $Al_{70}Co_{15}Ni_{14.9}Fe_{0.1}$ [25] quasicrystals, and amorphous $Zr_{65}Al_{7.5}Ni_{10}Cu_{7.3}Fe_{0.2}Ag_{10}$ [26]. The value of $\Delta(0)$ is close to the calculated value of 0.0921 mm/s.

The Mössbauer spectra of $Rb_{1-\delta}EuFe_4As_4$ at 20.2 and 16.4 K are compared in Fig. 7(b). One observes that the 16.4 K spectrum is slightly, but visibly, broader than the 20.2 K spectrum. This 0.014 mm/s broadening [Fig. 7(b)] over a very narrow temperature range of 3.8 K is the consequence of the appearance at 16.4 K of a very small H_{hf}. We surmise that this H_{hf} is transferred to the ^{57}Fe nuclei from the ferromagnetically ordered Eu sublattice (see below). A *transferred* hyperfine magnetic field at a given Mössbauer nucleus results from the neighboring magnetic moments [27]. It should be stressed that this transferred hyperfine magnetic field does not result from the ordering of the Fe sublattice. Its presence constitutes direct evidence of the ordering of the Eu sublattice. Such a transferred hyperfine magnetic field at a single temperature was observed first in the $EuFe_2(As_{1-x}P_x)_2$ superconductors [28]. Thus, the Mössbauer spectra at 16.4 K and lower temperatures were fitted (Fig. 8) with a large-spectral-area Zeeman pattern component [the value of Δ was fixed in the fit to that obtained from the fit of the $\Delta(T)$ dependence in Fig. 7(a)] that originates from $Rb_{1-\delta}EuFe_4As_4$ and with a small-spectral-area Zeeman pattern component that is due to the FeAs impurity phase.

Figure 9 displays the temperature dependence of the transferred H_{hf} that was derived from the fits of the spectra in Fig. 8.

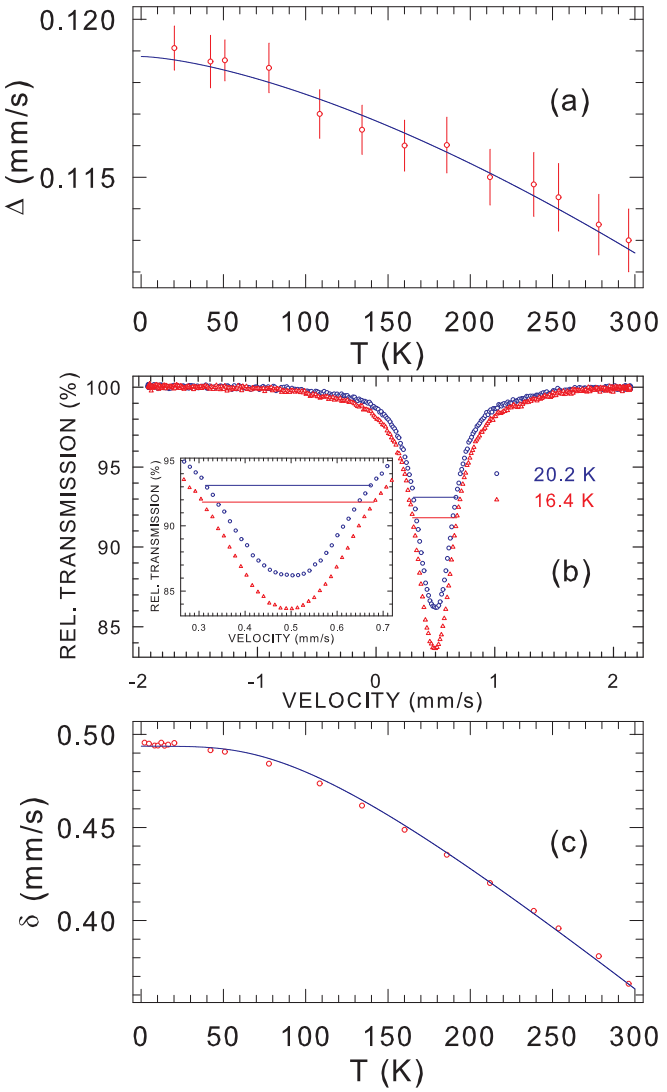

FIG. 7. (a) Temperature dependence of the quadrupole splitting. The solid line is the fit to Eq. (1), as explained in the text. (b) Comparison of the ^{57}Fe Mössbauer spectra of $Rb_{1-\delta}EuFe_4As_4$ at 20.2 and 16.4 K. The inset shows the spectra with enlarged horizontal and vertical scales. The horizontal bars indicate the full width at half maximum of the 20.2 K spectrum (0.359 mm/s) and the 16.4 K spectrum (0.373 mm/s). The zero-velocity origin is relative to α-Fe at room temperature. (c) Temperature dependence of the center shift δ. The solid line is the fit to the equation $\delta(T) = \delta_0 + \delta_{SOD}(T)$, as explained in the text.

As expected, H_{hf} increases with decreasing temperature. The $H_{hf}(T)$ dependence was fitted using the phenomenological form [29]

$$H_{hf}(T) = H_{hf}(0)\left[1 - \left(\frac{T}{T_C}\right)^{\alpha}\right]^{\beta}, \qquad (2)$$

where $H_{hf}(0)$ is the value of H_{hf} at 0 K and α and β are exponents describing the behavior of $H_{hf}(T)$ near 0 K and T_C, respectively. The fit yields $H_{hf}(0) = 6.17(2)$ kOe, $T_C = 16.63(16)$ K, $\alpha = 1.96(10)$, and $\beta = 0.21(2)$. The values of α and β found here are comparable to those obtained for other compounds [30–32].

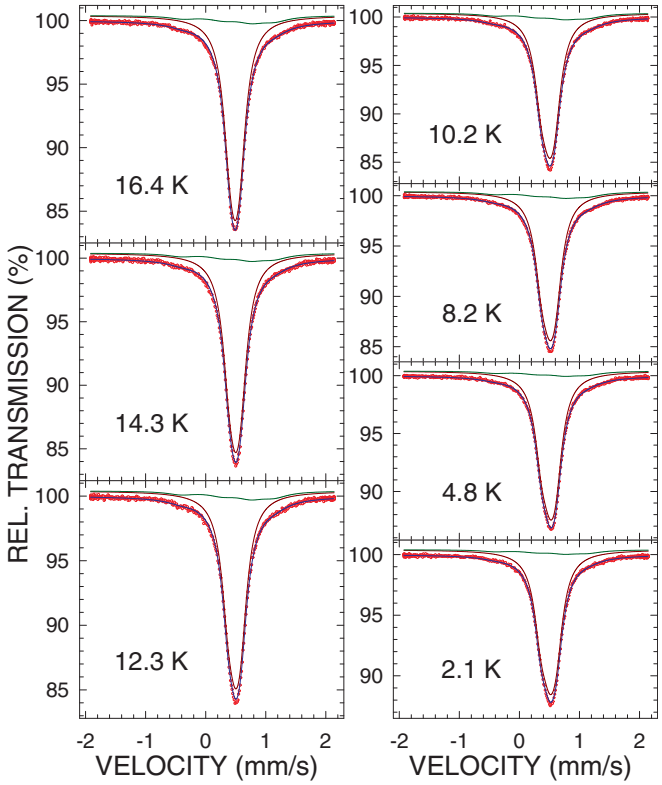

FIG. 8. ^{57}Fe Mössbauer spectra of $Rb_{1-\delta}EuFe_4As_4$ at the indicated temperatures fitted (solid blue lines) with a large-spectral-area Zeeman pattern due to $Rb_{1-\delta}EuFe_4As_4$ (dark red solid lines) and a small-spectral-area Zeeman pattern originating from the FeAs impurity phase (solid dark green lines), as described in the text. The zero-velocity origin is relative to α-Fe at room temperature.

The calculations predict a nonzero, but small, value of $|H_{hf}(0)|$ at the ^{57}Fe nuclei and of the magnetic moment carried by the Fe atoms μ_{Fe} (see above). This is at odds with the experimentally observed zero value of the intrinsic, i.e., not transferred, H_{hf} down to 2.1 K and, consequently, the zero value of μ_{Fe}. The failure of theory in predicting the zero values

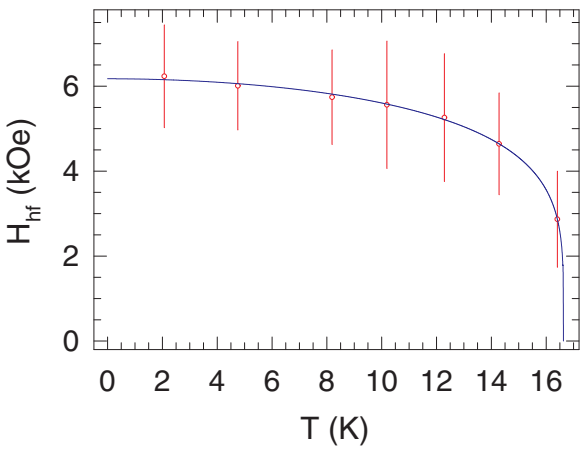

FIG. 9. Temperature dependence of the transferred hyperfine magnetic field. The solid line is the fit to Eq. (2), as explained in the text.

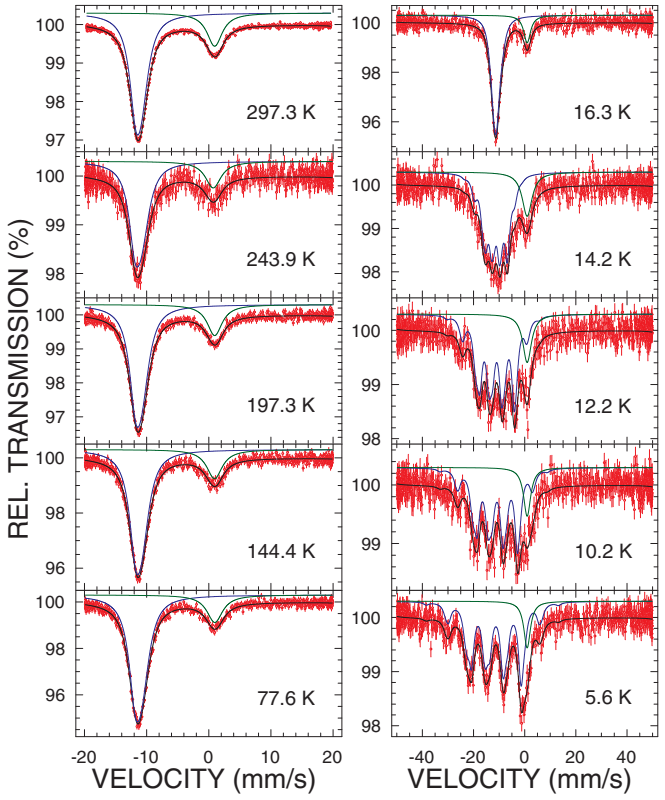

FIG. 10. ^{151}Eu Mössbauer spectra of $Rb_{1-\delta}EuFe_4As_4$ in the paramagnetic temperature region (left column) and the magnetic temperature region (right column). They are fitted (solid black lines) with a large-spectral-area quadrupole pattern (left column) and a large-spectral-area Zeeman pattern (right column) due to $Rb_{1-\delta}EuFe_4As_4$ (blue solid lines) and a small-spectral-area singlet originating from the Eu_2O_3 impurity phase (solid dark green lines), as described in the text. The zero-velocity origin is relative to the source.

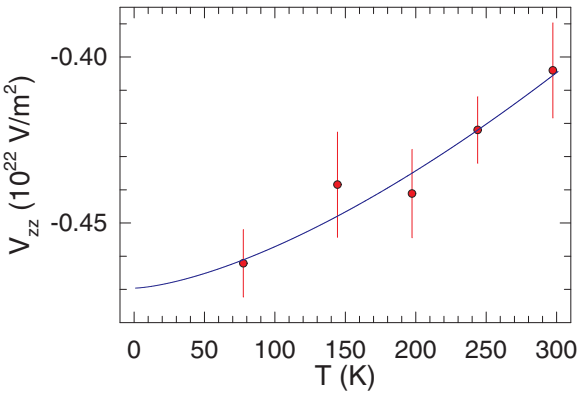

FIG. 11. Temperature dependence of the principal component of the electric-field-gradient tensor V_{zz} derived from the fits of the spectra in Fig. 10 (left column). The solid line is the fit to an empirical $T^{3/2}$ power-law relation, as explained in the text.

of H_{hf} and μ_{Fe} may be related to the inherent limitations of standard density functional theory, especially as applied to the strongly correlated systems or the d- or f-electron compounds with localized electrons [33].

The temperature dependence of the center shift δ that was obtained from the fits of the spectra in Figs. 5, 6, and 8, is shown in Fig. 7(c). The center shift at temperature T, $\delta(T)$, consists of two terms, $\delta(T) = \delta_0 + \delta_{SOD}(T)$, where δ_0 is the intrinsic, temperature-independent isomer shift and $\delta_{SOD}(T)$ is the second-order Doppler (SOD) shift. The latter is the function of the Debye temperature Θ_D [5]. The fit of the experimental data $\delta(T)$ [Fig. 7(c)] gives $\delta_0 = 0.494(2)$ mm/s and $\Theta_D = 391(8)$ K. We note that the experimental value of δ_0 found here is 30% larger than the calculated δ_0.

E. ^{151}Eu Mössbauer spectroscopy

The ^{151}Eu Mössbauer spectra of $Rb_{1-\delta}EuFe_4As_4$ at temperatures between room and liquid-helium temperatures are shown in Fig. 10. The spectra in the paramagnetic temperature region (left column in Fig. 10) consist of a large-spectral-area component in the form of an unresolved quadrupole octet [5,34] that originates from Eu^{2+} ions in $Rb_{1-\delta}EuFe_4As_4$ and a small-spectral-area component in the form of a single line due to Eu^{3+} ions in the Eu_2O_3 impurity phase. The spectral weight of the latter component is 22(1)% and is larger than that expected from the amount of 0.7(2) wt% of the Eu_2O_3 impurity derived from the Rietveld refinement of the x-ray diffraction spectrum. The Eu atoms in $Rb_{1-\delta}EuFe_4As_4$ are located at the $1a$ site with the point symmetry $4/mmm$ (Table I), which ensures an axially symmetric ($\eta = 0$) EFG tensor at this site. Also, V_{zz} is parallel to the c axis. The temperature dependence of V_{zz} derived from the fits of the spectra in the paramagnetic temperature region is shown in Fig. 11. Similar to the $\Delta(T)$ dependence in Fig. 7(a), the magnitude of V_{zz} increases with decreasing temperature. The $V_{zz}(T)$ data can be fitted to the same empirical $T^{3/2}$ power-law relation [Eq. (1)] in which $\Delta(T)$ and $\Delta(0)$ are replaced with $V_{zz}(T)$ and $V_{zz}(0)$, respectively. The fit of the $V_{zz}(T)$ data (Fig. 11) yields $V_{zz}(0) = -0.470(6)\times10^{22}$ V/m^2 and $B = 2.66(42)\times10^{-5}$ K$^{-3/2}$. The experimental value of $V_{zz}(0)$ compares very well with the calculated value of -0.497×10^{22} V/m^2.

The spectra in the magnetic temperature region (right column in Fig. 10) were fitted with a large-spectral-area Zeeman pattern component that originates from $Rb_{1-\delta}EuFe_4As_4$ and a small-spectral-area single-line component due to an impurity phase. The value of V_{zz} was fixed in the fit to that obtained from the fit of the $V_{zz}(T)$ dependence in Fig. 10. The temperature dependence of H_{hf} determined from the fits of these Mössbauer spectra is shown in Fig. 12(a). It is usually assumed that the temperature variation of H_{hf} in a magnetically ordered material can be reasonably explained within the framework of the molecular field model, assuming that H_{hf} is proportional to the sublattice magnetization. In terms of this model, $H_{hf}(T)$ can be expressed as

$$H_{hf}(T) = H_{hf}(0)B_J(x), \quad (3)$$

where $H_{hf}(0)$ is the saturation hyperfine magnetic field; $B_J(x)$ is the Brillouin function, defined as

$$B_J(x) = \frac{2J+1}{2J}\coth\left(\frac{2J+1}{2J}x\right) - \frac{1}{2J}\coth\left(\frac{x}{2J}\right); \quad (4)$$

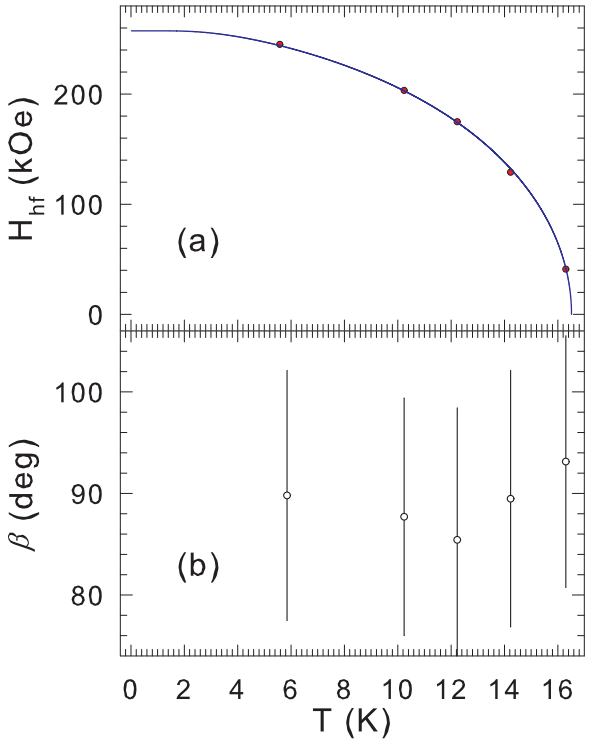

FIG. 12. Temperature dependence of (a) the hyperfine magnetic field H_{hf} and (b) the angle β determined from the fits of the spectra in Fig. 10 (right column). The solid line in (a) is the fit to Eq. (3), as explained in the text.

and

$$x = \frac{3J}{J+1}\frac{H_{hf}(T)}{H_{hf}(0)}\frac{T_C}{T}. \quad (5)$$

The fit of the $H_{hf}(T)$ data [Fig. 12(a)] to Eq. (3) with $J = S = 7/2$ (corresponding to a free Eu^{2+} ion) yields $H_{hf}(0) = 257.4(4.3)$ kOe and $T_C = 16.51(10)$ K. The T_C found here is very close to the value of 16.63(16) K derived from the temperature dependence of the transferred H_{hf} at ^{57}Fe nuclei. We take a weighted average of these two T_C values, 16.54(8) K, as the T_C of the studied superconductor. The experimental value of $H_{hf}(0)$ is significantly smaller than the calculated Fermi contact value of 483 kOe. This discrepancy can be explained by the fact that the measured hyperfine magnetic field at the ^{151}Eu nuclei is divided into three equally important contributions: $H_{hf} = H_c + H_{op} + H_n$. Here H_c is the core-polarization field (the Fermi contact term), H_{op} is due to conduction-electron polarization by the ion itself, and H_n includes all contributions from neighboring magnetic ions [35]. Clearly, the latter two contributions when added to the Fermi contact term must account for the measured $H_{hf}(0)$. Often, the H_{op} contribution has a sign opposite to that of the H_c contribution [34,35].

For ^{151}Eu Mössbauer spectroscopy [34,35], as opposed to ^{57}Fe Mössbauer spectroscopy [36], there is no simple relation between the measured $H_{hf}(0)$ and the magnetic moment carried by Eu atoms. We note here that the calculated Eu magnetic moment of $6.7095\mu_B$ is slightly larger than the experimental moment of $6.0\mu_B$ at 2 K [Fig. 3(b)].

The temperature dependence of the angle β (the angle between V_{zz} and H_{hf}) determined from the fits of the spectra in the magnetic temperature region (right column in Fig. 10) is shown in Fig. 12(b). One observes that the β values are close to 90°. This constitutes experimental proof that the Eu magnetic moments are perpendicular to the crystallographic c axis, that is, that they lie in the ab plane.

F. Discussion summary

A previous study concluded that $RbEuFe_4As_4$ bears both superconductivity and Eu-spin ferromagnetism but without any information about the Eu-spin direction [3]. Here, using the local-probe technique of Mössbauer spectroscopy, we have demonstrated that the Eu magnetic moments lie within the ab plane, akin to the case of nondoped $EuFe_2As_2$ in which an A-type antiferromagnetic (i.e., in-plane ferromagnetic but interplane antiferromagnetic) ordering occurs at 19 K [37–39]. Since $RbEuFe_4As_4$ can be viewed as a modified $EuFe_2As_2$ in which every other Eu layer is replaced by a Rb layer [Fig. 2(b)], one naturally expects that the Eu-layer spins in $RbEuFe_4As_4$ will become ferromagnetically ordered. Furthermore, the Eu spins are likely to be in the same direction as the Eu spins in $EuFe_2As_2$, i.e., along the crystallographic [110] direction [38,39]. We note that the Eu-spin direction in $RbEuFe_4As_4$ is in sharp contrast to the corresponding direction in doped $EuFe_2As_2$ systems where the Eu magnetic moments are basically along the c axis [28,40,41]. This phenomenon calls for a theoretical explanation.

The previous demonstration of the Eu-spin ferromagnetism is based mainly on the isothermal magnetization curves [3]. However, there could be a possibility that the observed ferromagnetism is field induced. In other words, the zero-field state may not necessarily be ferromagnetic. The present study rules out such a possibility because, at zero field, the ^{57}Fe nuclei feel the transferred hyperfine magnetic field $H_{hf}(0) = 6.17(2)$ kOe that results from the Eu-spin ferromagnetism. Indeed, the Eu-spin ferromagnetic polarization gives rise to an internal magnetic field of 4.5 kOe, which is close to the value of $H_{hf}(0)$.

IV. CONCLUSIONS

We presented the results of *ab initio* hyperfine-interaction parameters calculations and of x-ray diffraction and ^{57}Fe and ^{151}Eu Mössbauer spectroscopy study of the new 35.5 K superconductor $Rb_{1-\delta}EuFe_4As_4$. We confirmed that the superconductor crystallizes in the tetragonal space group $P4/mmm$ with the lattice parameters $a = 3.8847(1)$ Å and $c = 13.3370(3)$ Å. We showed that the Fe atoms carry no magnetic moment down to 2.1 K and that the ferromagnetic order is associated with the Eu magnetic moments. The Curie temperature $T_C = 16.54(8)$ K is determined from the temperature dependence of both the hyperfine magnetic field at ^{151}Eu nuclei and the transferred hyperfine magnetic field at ^{57}Fe nuclei that is induced by the ferromagnetically ordered Eu sublattice. We found that the Eu magnetic moments lie in the ab plane. We observed that the temperature dependence of the principal component of the electric-field-gradient tensor is well described by a $T^{3/2}$ power-law relation at both the Fe and Eu sites. Good agreement was found between the calculated and measured hyperfine-interaction parameters. We determined that the Debye temperature of $Rb_{1-\delta}EuFe_4As_4$ is 391(8) K.

ACKNOWLEDGMENT

This work was supported by the Natural Sciences and Engineering Research Council of Canada (NSERC) and the National Natural Science Foundation of China (Grant No. 11474252).

[1] A. Iyo, K. Kawashima, T. Kinjo, T. Nishio, S. Ishida, H. Fujihisa, Y. Gotoh, K. Kihou, H. Eisaki, and Y. Yoshida, J. Am. Chem. Soc. **138**, 3410 (2016).

[2] K. Kawashima, T. Kinjo, T. Nishio, S. Ishida, H. Fujihisa, Y. Gotoh, K. Kihou, H. Eisaki, Y. Yoshida, and A. Iyo, J. Phys. Soc. Jpn. **85**, 064710 (2016).

[3] Y. Liu, Y.B. Liu, Z.-T. Tang, H. Jiang, Z.-C. Wang, A. Ablimit, W.-H. Jiao, Q. Tao, C.-M. Feng, Z.-A. Xu, and G.-H. Cao, Phys. Rev. B **93**, 214503 (2016).

[4] Y. Liu, Y.-B. Liu, Q. Chen, Z.-T. Tang, W.-H. Jiao, Q. Tao, Z.-A. Xu, and G.-H. Cao, Sci. Bull. **61**, 1213 (2016).

[5] N. N. Greenwood and T. C. Gibb, *Mössbauer Spectroscopy* (Chapman and Hall, London, 1971); P. Gütlich, E. Bill, and A. Trautwein, *Mössbauer Spectroscopy and Transition Metal Chemistry* (Springer, Berlin, 2011).

[6] Y. Tanaka, R. M. Steffen, E. B. Shera, W. Reuter, M. V. Hoehn, and J. D. Zumbro, Phys. Rev. C **29**, 1830 (1984).

[7] I. Nowik and I. Felner, Hyperfine Interact. **28**, 959 (1986).

[8] *Certificate of Calibration, Iron Foil Mössbauer Standard*, edited by J. P. Cali, Natl. Bur. Stand. (US) Circ. 1541 (1971).

[9] S. Margulies and J. R. Ehrman, Nucl. Instrum. Methods **12**, 131 (1961); G. K. Shenoy, J. M. Friedt, H. Maletta, and S. L. Ruby, in *Mössbauer Effect Methodology*, edited by I. J. Gruverman, C. W. Seidel, and D. K. Dieterly (Plenum, New York, 1974), Vol. 10, p. 277.

[10] P. Blaha, K. Schwartz, G. Madsen, D. Kvasnicka, and J. Luitz, *WIEN2k: An Augmented Plane Wave Plus Local Orbitals Program for Calculating Crystal Properties* (Technische Universität Wien, Austria, 2001).

[11] F. Nejadsattari, P. Wang, Z. M. Stadnik, Y. Nagata, and T. Ohnishi, J. Alloys Compd. **725**, 1098 (2017).

[12] R. A. Young, *The Rietveld Method* (Oxford University Press, Oxford, 1993).

[13] K. Selte, A. Kjekshus, and A. F. Andersen, Acta Chem. Scand. **26**, 3101 (1972).

[14] G. Martínez-Pinedo, P. Schwerdtfeger, E. Caurier, K. Langanke, W. Nazarewicz, and T. Söhnel, Phys. Rev. Lett. **87**, 062701 (2001).

[15] P. Blaha, J. Phys.: Conf. Ser. **217**, 012009 (2010).

[16] U. D. Wdowik and K. Ruebenbauer, Phys. Rev. B **76**, 155118 (2007).

[17] A. J. Freeman and R. E. Watson, Phys. Rev. **131**, 2566 (1963).

[18] S. K. Kulshreshtha and P. Raj, J. Phys. F **9**, 2253 (1979).

[19] L. Häggström, A. Gustavsson-Seidel, and H. Fjellvåg, Europhys. Lett. **9**, 87 (1989).

[20] A. Błachowski, K. Ruebenbauer, J. Żukrowski, and Z. Bukowski, J. Alloys. Compd. **582**, 167 (2014).

[21] M. A. Albedah, F. Nejadsattari, Z. M. Stadnik, Z.-C. Wang, C. Wang, and G.-H. Cao, J. Alloys Compd. **695**, 1128 (2017)

[22] F. Nejadsattari, Z. M. Stadnik, J. Przewoźnik, and B. Grushko, J. Alloys Compd. **662**, 612 (2016).

[23] M. A. Albedah, F. Nejadsattari, Z. M. Stadnik, and J. Przewoźnik, J. Alloys Compd. **619**, 839 (2015).

[24] Z. M. Stadnik and P. Wang, J. Phys.: Condens. Matter **18**, 8383 (2006).

[25] Z. M. Stadnik and G. Zhang, J. Phys.: Condens. Matter **16**, 7303 (2004).

[26] Z. M. Stadnik, Ö. Rapp, V. Srinivas, J. Saida, and A. Inoue, J. Phys.: Condens. Matter **14**, 6883 (2002).

[27] W. Zinn, J. Phys. (Paris) Colloq. **32**, C1-724 (1971); Ch. Sauer, U. Köbler, W. Zinn, and G. M. Kalvius, *ibid.* **35**, C6-269 (1974); G. Czjzek, V. Oestreich, H. Schmidt, K. Łątka, and K. Tomala, J. Magn. Magn. Mater. **79**, 42 (1989); I. Nowik, Y. Levi, I. Felner, and E. R. Bauminger, *ibid.* **147**, 373 (1995).

[28] I. Nowik, I. Felner, Z. Ren, G. H. Cao, and Z. A. Xu, J. Phys.: Condens. Matter **23**, 065701 (2011).

[29] S. J. Blundell, C. A. Steer, F. L. Pratt, I. M. Marshall, W. Hayes, and R. C. C. Ward, Phys. Rev. B **67**, 224411 (2003).

[30] P. J. Baker, I. Franke, T. Lancaster, S. J. Blundell, L. Kerslake, and S. J. Clarke, Phys. Rev. B **79**, 060402(R) (2009).

[31] P. J. Baker, H. J. Lewtas, S. J. Blundell, T. Lancaster, I. Franke, W. Hayes, F. L. Pratt, L. Bohaty, and P. Becker, Phys. Rev. B **81**, 214403 (2010).

[32] Z. Li, Y. Fang, X. Ma, H. Pang, and F. Li, Phys. Rev. B **84**, 134509 (2011).

[33] W. Chibani, X. Ren, M. Scheffler, and P. Rinke, Phys. Rev. B **93**, 165106 (2016), and references therein; T. Schickling, J. Bünemann, F. Gebhard, and L. Boeri, *ibid.* **93**, 205151 (2016), and references therein; K. Cao, H. Lambert, P. G. Radaelli, and F. Giustino, *ibid.* **97**, 024420 (2018), and references therein.

[34] F. Grandjean and G. L. Long, in *Mössbauer Spectroscopy Applied to Inorganic Chemistry*, edited by G. J. Long and F. Grandjean (Plenum, New York, 1989), Vol. 3, p. 513, and references therein.

[35] I. Nowik, B. D. Dunlap, and J. H. Wernick, Phys. Rev. B **8**, 238 (1973).

[36] F. Nejadsattari, Z. M. Stadnik, J. Przewoźnik, and K. H. J. Buschow, Phys. B (Amsterdam, Neth.) **477**, 113 (2015), and references therein.

[37] S. Jiang, Y. Luo, Z. Ren, Z. Zhu, C. Wang, X. Xu, Q. Tao, G. Cao, and Z. Xu, New J. Phys. **11**, 025007 (2009).

[38] J. Herrero-Martín, V. Scagnoli, C. Mazzoli, Y. Su, R. Mittal, Y. Xiao, T. Brueckel, N. Kumar, S. K. Dhar, A. Thamizhavel, and L. Paolasini, Phys. Rev. B **80**, 134411 (2009).

[39] Y. Xiao, Y. Su, M. Meven, R. Mittal, C. M. N. Kumar, T. Chatterji, S. Price, J. Persson, N. Kumar, S. K. Dhar, A. Thamizhavel, and Th. Brueckel, Phys. Rev. B **80**, 174424 (2009).

[40] W. T. Jin, S. Nandi, Y. Xiao, Y. Su, O. Zaharko, Z. Guguchia, Z. Bukowski, S. Price, W. H. Jiao, G. H. Cao, and Th. Brückel, Phys. Rev. B **88**, 214516 (2013).

[41] S. Nandi, W. T. Jin, Y. Xiao, Y. Su, S. Price, D. K. Shukla, J. Strempfer, H. S. Jeevan, P. Gegenwart, and Th. Brückel, Phys. Rev. B **89**, 014512 (2014).